

Strontium Titanate (SrTiO₃) Mesoporous Coatings for Enhanced Strontium Delivery and Osseointegration on Bone Implants

Ane Escobar, Nicolás Muzzio, Paula C. Angelomé, Andrea V. Bordoni, Angel Martínez, Elisa Bindini, Emerson Coy, Patrizia Andreozzi, Marek Grzelczak, and Sergio E. Moya*

The incorporation of strontium (Sr) in titania enhances surface bioactivity and has a positive effect on pre-osteoblastic cell attachment, proliferation, and differentiation. Strontium titanate mesoporous films (SrTiMFs) with 30% pore volume and a 20% Sr molar content have been prepared by the evaporation induced self-assembly method. SrTiMFs display a large internal surface area available for exchange of Sr, which is released in cell media up to 44% within the first 8 h. SrTiMFs improve attachment of MC3T3-E1 pre-osteoblastic cells, which show larger filopodia and more elongated features than cells attached to plain mesoporous titania films (MTFs). SrTiMFs also display improved cell proliferation and differentiation rates indicating that overall Sr incorporation into mesoporous titania coatings can lead to enhanced osseointegration during the early stages of bone tissue formation.

1. Introduction

Among a vast number of available materials, titanium and its alloys are the most used materials for orthopedic implants.^[1–3] The increased use of titanium and titanium alloys as biomaterials is due to their superior biocompatibility and excellent corrosion resistance properties.^[4,5] Since the role of an implant is to replace bone, it needs to mimic the biological environment and mechanical properties of the bone. Depending on the type of bone, the elastic modulus varies between 4 and 30 GPa.^[6] Currently used commercial titanium implants satisfy the required mechanical properties with a Young's modulus within the range of 100–120 GPa.^[7] However, the surface characteristics of the titanium implants such as the topography and bioactivity can be considered sub-optimal

for cell adhesion and tissue formation. Several strategies have been proposed to improve interaction between titanium implants and the regenerating bone tissue.^[8–10] Implant surface topography plays an important role on the osseointegration process with cells adhering better to rougher surfaces. Indeed, titania with nanoscale surface features has been shown to favor osseointegration.^[11,12] To increase the bioactivity of titania, growth factors can be deposited on the implant or the titania can be doped with bioactive ions.^[13,14]

Several ions present in the human bone mineral apatites like calcium (Ca²⁺), magnesium (Mg²⁺), niobium (Nb⁵⁺), phosphate (PO₄³⁻), silicate (Si⁴⁺), strontium (Sr²⁺), and zinc (Zn²⁺) are known to promote osteoblastic precursor cell differentiation.^[15] The incorporation of some of these bioactive ions in titania, in particular Sr, has been shown to induce growth factor signaling pathways to osteoblastic precursor cell differentiation.^[16]


Approximately 98% of the Sr present in our body is localized in bone tissue^[17] where it has a beneficial effect on bone metabolism due to its anabolic and antiresorptive activity.^[18] Sr has been shown to be a promising therapeutic agent to heal bone disease, and strontium ranelate, for example, has been used in clinics for a long time.^[19] As oral medication strontium ranelate has been proved to act on both the desorption and formation of bone,^[20] but currently is not recommended due to the side effects it has when administered orally.^[21] These side effects are

Dr. S. E. Moya, Dr. A. Escobar, Dr. N. Muzzio, Dr. E. Bindini,
Dr. P. Andreozzi, A. Martínez
CIC biomaGUNE
Paseo de Miramón 182, 20014 Donostia-San Sebastián, Spain
E-mail: smoya@cicbiomagune.es

Dr. A. V. Bordoni, Dr. P. C. Angelomé
Gerencia Química – Centro Atómico Constituyentes
Comisión Nacional de Energía Atómica, CONICET
Avenida General Paz 1499, B1650KNA San Martín, Buenos Aires,
Argentina

Dr. E. Coy
NanoBioMedical Center
Adam Mickiewicz University
ul. Wszechnicy Piastowskiej 3, 61-614 Poznań, Poland

Dr. M. Grzelczak
Ikerbasque
Basque Foundation for Science
48013 Bilbao, Spain
Donostia International Physics Center
Paseo de Manuel Lardizabal 4
20018 Donostia-San Sebastián, Spain

 The ORCID identification number(s) for the author(s) of this article can be found under <https://doi.org/10.1002/adem.201801210>.

DOI: 10.1002/adem.201801210

suppressed when the drug is locally administered.^[22] Sr itself promotes osteogenic differentiation of mesenchymal stem cells by up-regulating the expression of osteoblast marker genes, such as *Runx2*, osteocalcin (*OCN*), osteopontin (*OPN*), bone sialoprotein (*BSP*), and type 1 collagen, and by increasing alkaline phosphatase activity and matrix mineralization.^[23]

Sr incorporated into titania has been shown to lead to an enhanced osseointegration and an improved differentiation of pre-osteoblastic cells.^[14,24] However, the incorporated Sr must be released into the environment of the regenerating tissue for a positive action. Besides the amount of Sr incorporated into the titania, the area available for ion exchange plays an important role in the release of Sr as it will only be delivered into the media when it is located on the surface.^[14,25] Rougher titania surfaces, for example, have been shown to deliver Sr more effectively than plain titania as a consequence of the larger available surface area.^[14,16,26] A possible means to increase the surface area for ion delivery is the use of mesoporous titania. Mesoporous materials have an ordered, homogenous array of pores with highly controlled diameters in the 2–10 nm range.^[27] Titania can be synthesized as a mesoporous material without compromising its mechanical properties,^[28] which is fundamental for bone replacement. Moreover, a mesoporous titania film (MTF) can be easily synthesized on top of non-porous titania with the same biocompatibility properties as the non-porous titania.

A large surface area is available in mesoporous films that can be used for the delivery of Sr or other bioactive element present in the formulation of the mesoporous material.^[29] The larger surface area results in a larger amount of Sr potentially available for delivery in the media compared with non-porous titania with the same Sr content. Moreover, the mesoporous material can be designed to present interconnected pores linked by narrow necks. Once the Sr is released from the surface of the pore it will have to escape through the pores, retarding its release from the film, which could enhance its therapeutic effect. Importantly, it is possible to incorporate Sr or Ca into the MTF during the synthesis process simply by adding ionic salts to the sol, as demonstrated by Grandfield et al.^[30] This way the ions could be incorporated into the titania matrix, up to a Sr:Ti molar ratio of 0.01:1.^[30] Strontium salts are not very soluble,^[31–33] and depending on the synthetic pathway and solvents used to obtain the mesoporous films, the concentration of the Sr salt that can be incorporated during the synthesis varies. Grosso et al.^[34] also incorporated Sr in MTFs and found a 1:1 Sr:Ti ratio but only in nanocrystals located in the walls of the mesoporous structure, thus lacking a homogeneous Sr distribution.^[34]

For this work, we prepared strontium titanate mesoporous films (SrTiMFs) by sol–gel chemistry and report here on their structural and mechanical properties, and their bioactivity in pre-osteoblastic cell culture.

2. Results and Discussion

2.1. SrTiMF Synthesis and Functionalization

SrTiMFs are synthesized by sol–gel chemistry applying the evaporation-induced self-assembly process. The block copolymer Pluronic F127[®] was used to generate the mesoporous structure. Transmission electron microscopy (TEM) and scanning electron microscopy (SEM) imaging confirmed the porous structure (Figure 1a and b). The pore ordering is not well defined; some regions present disordered pores, while others appear to have well-ordered pores with an array similar to the typical body centered cubic array of mesopores seen in F127 templated oxides. The SAXS pattern of the SrTiMF, taken at 90° shows a circular pattern compatible with MTFs in which pores in the *xy* plane are polyoriented, matching what is observed by electron microscopy (Figure 1a, inset).^[35] The calculated interplanar (–110) distance from the SAXS pattern is 11.1 nm, typical of F127 templated mesoporous oxides.^[36] Water adsorption and desorption isotherms (Figure 1c) indicate a porous volume of 30% and a pore diameter of 5.5 nm. The bottlenecks connecting the pores have a diameter of 3.2 nm, and the SrTiMF film thickness is 85 nm. These results also confirm that the inner porous volume of the film is accessible to water. In these conditions, Sr present in the walls could come into contact with cell media and be released. Due to their high porous volume, SrTiMFs have a much larger surface area compared with non-

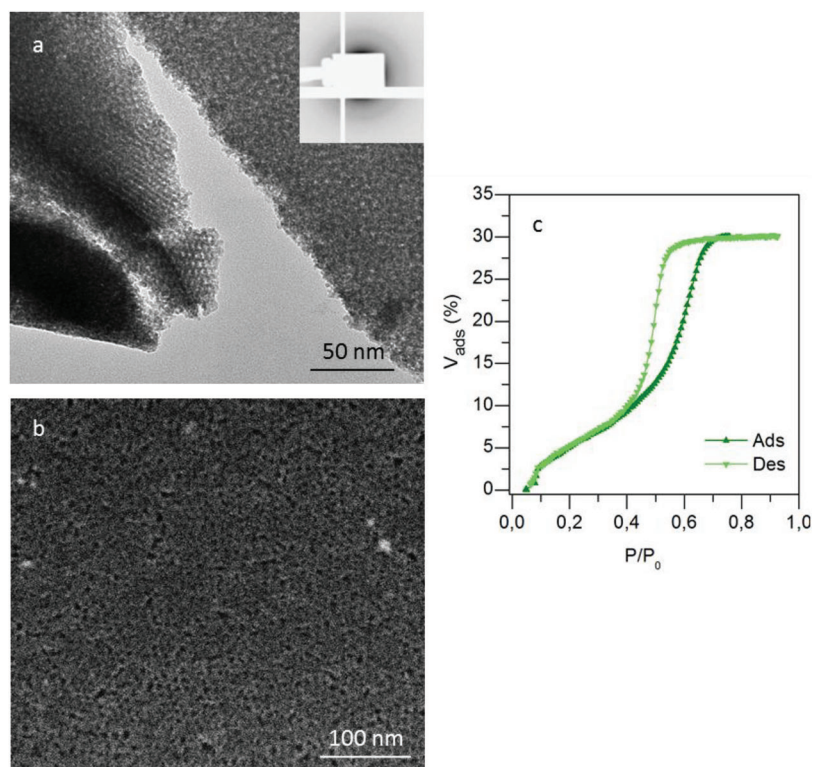


Figure 1. SrTiMF structural characterization by electron microscopy, SAXS and EEP. a) TEM image in which the pores in the film appear as white spots; insert: 2D-SAXS pattern taken at 90° indicating a film with polyoriented pores, b) SEM image of the surface in which pores appear as dark spots and c) water adsorption-desorption isotherm, obtained by EEP.

porous titania films.^[37] This characteristic could allow for greater release of Sr from the surface when in contact with cell media. Sangle et al.^[38] synthesized mesoporous SrTiO₃ films by pulse laser deposition and obtained rod-like mesoporous structures of 20 nm with a wall thickness of 5–7 nm. When films are around 100 nm thick, the surface area is increased by 2500% compared with a non-porous surface of same dimensions.^[38]

Nanoindentation measurements (Figure S1) showed an elastic modulus of 25 ± 5 GPa for the MTF (Figure S1b) and 35 ± 7 GPa for the SrTiMF (Figure S1c). This result indicates that the elastic modulus of the MTFs is slightly affected by the incorporation of Sr into the mesoporous structure. This small increment can be associated to several aspects, including the higher elastic modulus and density of SrTiO₃ (185 ± 15 GPa and 5.11 g cm⁻³) when compared with TiO₂ (110 ± 10 GPa and 4.23 g cm⁻³); additionally, the changes in porosity of the SrTiMFs with respect of the undoped MTFs are negligible, which supports the small reinforcement in the porous structure by Sr doping.

In addition, the study of the mechanical stability and nanotribological of the surfaces (Figure S1d), showed that SrTiMFs samples have slightly superior wear resistance (1.1 μm³) and lower friction coefficient (0.34 μ_B) than MTFs

(1.5 μm³ and 0.45 μ_B, respectively), hinting on the benefit of Sr doping on the mechanical properties of the samples, which although display a lower elasticity modulus than non porous TiO₂ (100 ± 10 GPa)^[7] remains within the range of the elasticity of different types of bones (4–30 GPa).^[6]

The Sr:Ti molar ratio in the film synthesis was 0.2:1, which was the highest one possible to obtain an optimal solution for synthesis. If the concentration of SrCl₂ was augmented, it started to precipitate resulting in an inhomogeneous solution. X-ray photoelectron spectroscopy (XPS) measurements confirmed that this ratio is retained after film synthesis, where the resulting relative Sr/Ti atomic percentage is around 20.8 ± 0.4%. Compared with Grandfield et al.^[30] who obtained a Sr:Ti molar ratio of 0.01:1, our SrTiMFs have 20 times more strontium incorporated into the film and, very importantly, in a homogeneous distribution.

XPS spectra of SrTiMFs confirm that Sr is integrated into the titanium network (Figure 2) determined by the notable absence of chlorine from the spectra (which should appear at 199 cm⁻¹), which indicates that Sr is not forming SrCl₂ crystals. Following digestion of the SrTiMF, the total amount of Sr in the film was 2.29 ± 0.53 μg, obtained by inductively coupled plasma mass spectrometry (ICP-MS) measurements of three samples.

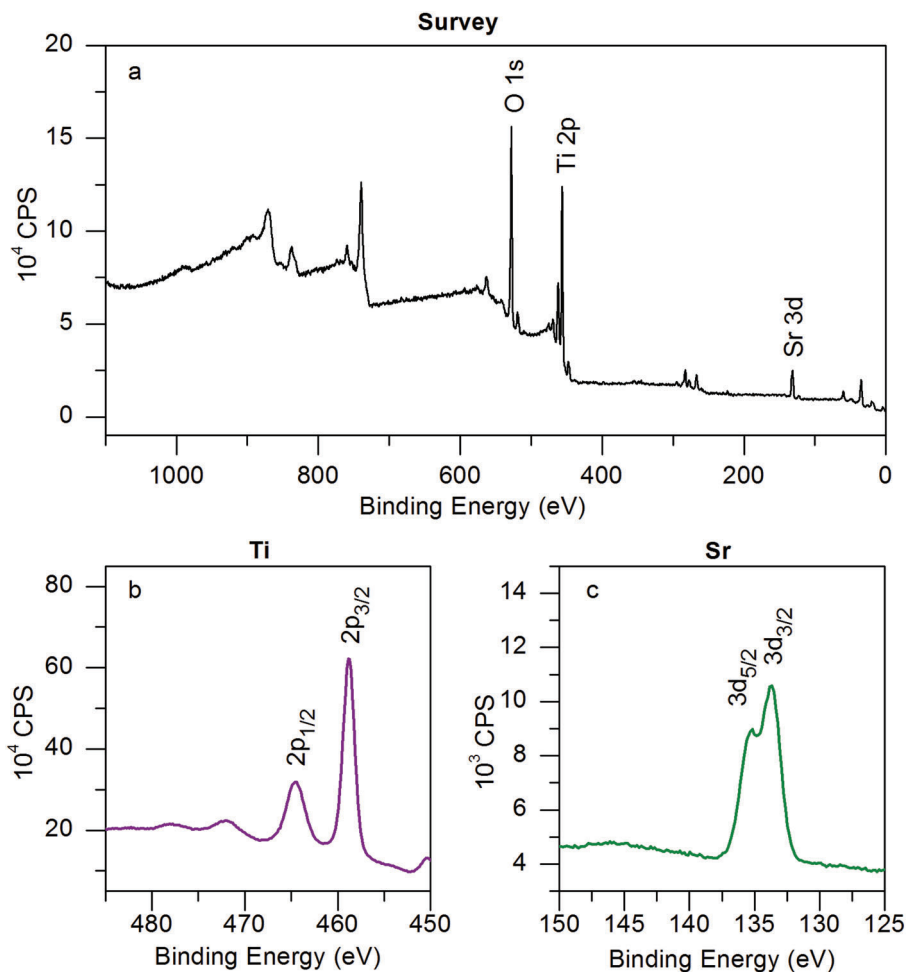


Figure 2. XPS a) survey spectra and high resolution spectra for b) Ti and c) Sr from SrTiMFs.

Scanning transmission electron microscopy (STEM) and energy dispersive X-ray analysis (EDX) performed at different regions of the SrTiMF confirm that Sr is homogeneously distributed throughout the mesoporous structure (Figure S2). EDX spectra obtained from three points in the same sample region show that there are no regions where Ti or Sr bands are missing, meaning that the mesoporous network has a homogeneous distribution of the elements and no phase segregation occurs in the mesoporous oxide (Figure S2c).

2.2. Strontium Release

The release profile of Sr measured by ICP-MS shows that $38.58 \pm 1.77\%$ of Sr is released after 1 h and $43.76 \pm 7.99\%$ is released after 8 h (Figure 3). The subsequent measurements at 24 h show that $44.41 \pm 6.61\%$ of Sr is released. The release curve indicates a fast release within the first 8 h, where the maximum release is reached, followed by a release that is very slow but continuous. The release characteristics of the mesoporous films could be further tuned by modifying the pore size, porous structure, or film thickness.^[37] The larger the surface area and thickness of the SrTiMF, the higher the concentration of ions available for release will be.^[37,39] When SrTiMFs are immersed for 24 h in 10 mM phosphate buffered saline (PBS), TEM imaging shows that the films do not suffer any noticeable dissolution and the porous structure is maintained without any appreciable changes (Figure S3).

2.3. Biocompatibility and Bioactivity Evaluation

Initial cell adhesion on biomaterials plays a key role on cell proliferation, migration, and differentiation. The focal adhesions

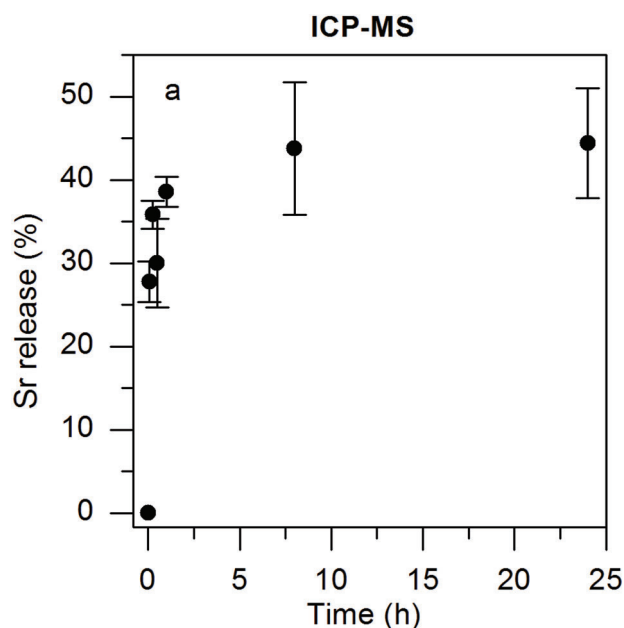


Figure 3. Percentage of Sr release from SrTiMFs over time measured with ICP-MS.

and extracellular matrix (ECM) interactions involve integrins that bind different ECM proteins with the external end and cytoskeleton via adapter proteins such as talin, α -actinin, filamin, and vinculin. The pathways involving these integrins can regulate subsequent cell adhesion, migration, proliferation, and differentiation.^[40]

Confocal laser scanning microscopy (CLSM) of MC3T3-E1 osteoblast precursor cells cultured on MTFs and SrTiMFs was used to evaluate cellular adhesion to the films (Figure 4 and S4). In the F-actin images, cells cultured on SrTiMFs exhibit a similar size as those grown on MTFs, and show an arranged cytoskeleton with distinctive stress fibers inside the cytoplasm, especially at the borders of the cells. However, after 48 h of culture, cells grown on SrTiMFs display a more elongated cell shape and increased filopodia compared with those grown on MTFs (Figure 4 and S4, third column). This difference implies that the presence of Sr improves the interaction between the cells and the film, facilitating good attachment of the cells to the film's surface. Vinculin interconnects signals in the focal adhesions and is a key regulator in environmental sensing.^[41] Vinculin, visualized in green, is clearly visible by CLSM and green dots can be distinguished at the end of the actin filaments of cells cultured on SrTiMFs (Figure 4, third and fourth rows). After 2 h of cell incubation on the substrates (Figure 4, first column) focal adhesions can be perfectly distinguished, demonstrating that cells adhere well to the substrates already at initial time points and that adhesion may later improve cell proliferation.^[42,43]

Cell proliferation was measured for MC3T3-E1 cells cultured on MTF and SrTiMF substrates (Figure 5). After 7 days, the culture is confluent, meaning that the surface is completely covered by cells forming a monolayer, and no difference can be distinguished between the samples. Within the first day of culture, cells proliferate at the same rate, and the cell density is similar for both substrates. After 2 days of culture, the cell proliferation rate on SrTiMFs is enhanced compared with cells cultured on MTFs ($p < 0.05$). After 2 days, the proliferation on SrTiMFs is 64% higher compared with that on MTFs, and after 3 days of culture the proliferation is 52% higher. As previously seen (Figure 4), cells are more expanded and show more filopodia, indicating better surface interaction, which is known to improve cell proliferation.^[42,43] These results confirm as expected that Sr enhances pre-osteoblastic cell proliferation.^[44] However, more importantly, the manner in which Sr is released from the mesoporous structure demonstrates that this substrate is a good candidate for enhancing cell attachment and proliferation at initial times after the implant is placed in the human body.

To assess cell differentiation on MTF and SrTiMF substrates, we measured the enzymatic activity of alkaline phosphatase, a well-established marker for the early stage of osteogenic differentiation.^[45] MC3T3-EC1 cells were cultured on MTFs or SrTiMFs. After cells reached confluence, they were differentiated for 20 days and the alkaline phosphatase activity was measured at various times to evaluate the degree of differentiation. Statistically significant differences ($p < 0.05$) between the substrates were observed starting from soon after the cells were cultured on the substrates, alkaline phosphatase activity is more than double for cells grown on SrTiMFs compared with

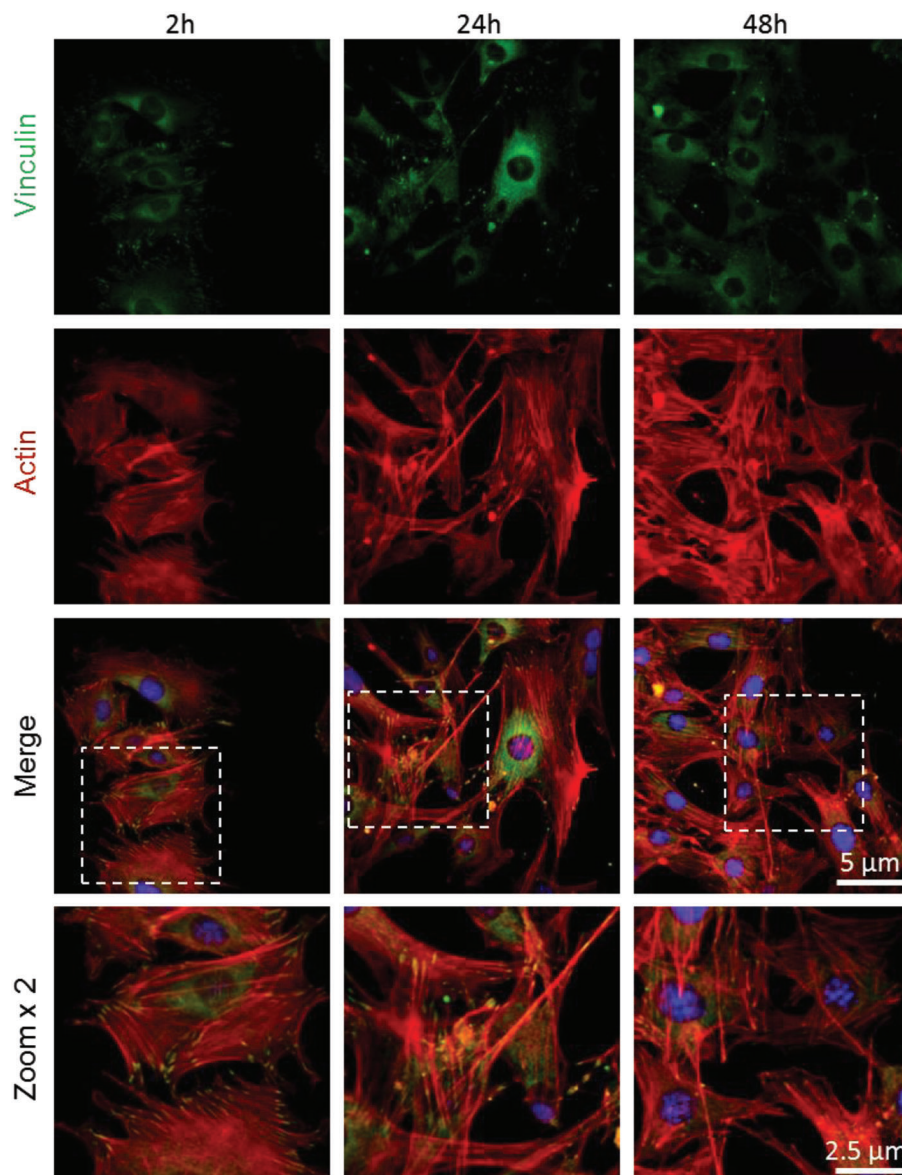


Figure 4. Confocal laser scanning microscopy images of vinculin (first row), actin (second row), the merge of actin, vinculin and the nucleus (third row) and the zoom of the merge image (fourth row) at 2 h (first column), 24 h (second column), and 48 h (third column) of growth of MC3T3-E1 cells on SrTiMF substrates at 63 \times . The actin filaments (F-actin) are stained with phalloidin, visible in red fluorescence; vinculin is stained with FITC, visible in green; and the nucleus is stained with DAPI, appearing in blue.

those grown on MTFs. Subsequent measurements at 10, 15, and 20 days also confirmed enhanced cell differentiation on SrTiMFs.

3. Conclusion

We have shown here that Sr can be incorporated into MTFs with a porous and accessible structure, and that the bioactive ions are homogeneously distributed in the MTFs. A 20% molar content of Sr has been achieved, the larger content reported for Sr incorporation into mesoporous titania. Due to the high porous volume of the SrTiMTF, around 30%, there is a large area for Sr

exchange, accessible to external fluids that leads to Sr release in the medium. At physiological pH in 10 mM PBS, 44% of the Sr present in the films is released over 8 h.

SrTiMFs improve MC3T3-E1 cell adhesion and proliferation if compared with TiMTFs. Cell differentiation is also enhanced by more than 100% after 5 days when Sr is present in the mesoporous structure.

To resume, we show here the synthesis of mesoporous titania films with a high Sr content and with a large surface area for ion exchange through the mesoporous structure. Films can be easily assembled on top of titania implants with a high potential for increasing osseointegration, especially in the early stages after implant surgery.

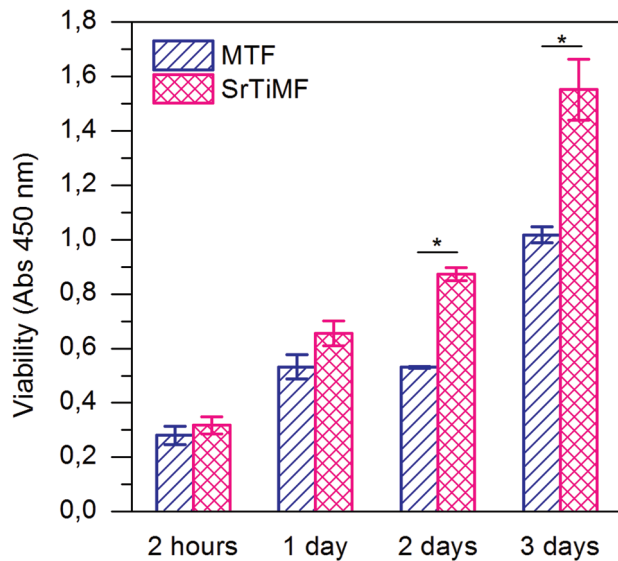


Figure 5. Proliferation of MC3T3-E1 pre-osteoblasts cultured on MTF and SrTiMF substrates for 2 h, and 1, 2, and 3 days. * indicates the difference is statistically significant ($p < 0.05$).

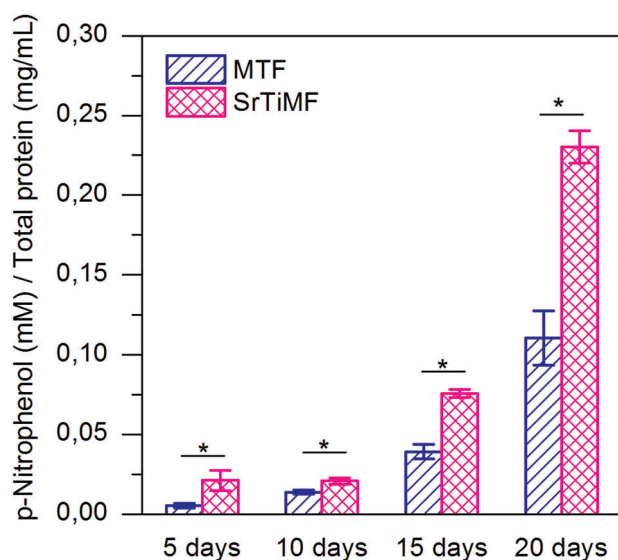


Figure 6. Alkaline phosphatase activity after 5, 10, 15, and 20 days of MC3T3-E1 pre-osteoblastic cell culture in osteogenic medium on MTF and SrTiMF substrates. * indicates the difference is statistically significant ($p < 0.05$).

4. Experimental Section

SrTiMF Synthesis: SrTiMFs with a pore diameter of 5.5 nm were synthesized by the evaporation induced self-assembly method. Films were prepared on round glass coverslips 14 mm in diameter and 0.13–0.16 mm in thickness from Thermo Scientific. Pluronic® F-127 (EO₁₀₆PO₇₀EO₁₀₆) was used as structure-directing agent.

For the sol preparation, titanium (IV) chloride ($\geq 99.0\%$, TiCl₄), strontium chloride hexahydrate (SrCl₂ × 6H₂O), absolute ethanol (synthesis grade, EtOH), Pluronic F-127, and nanopure water (H₂O)

were mixed in a molar ratio of TiCl₄:EtOH:SrCl₂:F-127:H₂O = 1:40:0.2:0.0056:10. The titania precursor was prepared first, adding TiCl₄ to the EtOH under vigorous stirring and leaving it until it dropped to room temperature. SrCl₂ was homogenized under stirring in water, then the F-127 was added under stirring and finally the titania precursor was added. The sol was left stirring for 10 min to obtain a homogenous solution.

For preparation of the films, 30 μ L of the sol was mixed with EtOH in a volume proportion of sol:EtOH = 2:1 and spin coated at 68 rpm for 30 s on glass coverslips. Films were placed for 30 min in a humidity chamber with a relative humidity of 50% and then subjected to a thermal treatment: 30 min at 60 °C and another 30 min at 130 °C. Finally, films were calcinated; first, heated up with a ramp of 1 °C min⁻¹ and then kept at 350 °C for 2 h. For use as controls, MTFs were synthesized following the same procedure but without adding SrCl₂.

Ethanol was purchased from Scharlau. All other reagents were purchased from Sigma–Aldrich. Prior to use samples were cleaned by immersing them in ethanol, then in water and leaving them to dry in air.

SrTiMF Characterization: For pore visualization, a JEOL JEM-1400PLUS transmission electron microscope equipped with a Gatan US1000 CCD camera was used. Films were scratched to obtain a powder, which was deposited on carbonated copper grids with a drop of pure ethanol. Film topology was visualized with a Carl Zeiss NTS Supra 40 field emission scanning electron microscope (FE-SEM) at the Advanced Microscopy Center FCEN-UBA (Argentina).

Ellipsometric and environmental ellipsometric porosimetry (EEP) measurements were performed with a UV-IR (193–1690 nm) variable angle spectroscopic ellipsometer (VASE) M2000DI from Woollam, using samples previously washed with absolute ethanol and dried. For EEP, film thickness and refractive index values are obtained from the ellipsometric parameters Ψ and Δ and samples are measured under dry air flux containing variable water vapor pressure P ; P/P_0 was varied from 0 to 1 (P_0 being the saturation water vapor pressure at 25 °C). Water volume adsorbed at each P/P_0 value was determined by modeling the obtained refractive index according to a three-component (water-air-oxide) Bruggeman effective medium approximation. Adsorption–desorption isotherms were obtained by plotting the water volume adsorbed to the porous film at each P/P_0 . The pore size distribution was obtained from the isotherms using the Kelvin equation, employing the value of P/P_0 at which water capillary condensation takes place within the pores and taking into account the water contact angle in the film.^[29] Water contact angles required for such calculations were determined using a drop shape analyzer DSA100 from Kruss.

2D-small angle X-ray scattering (SAXS) patterns were obtained at the Austrian SAXS beamline at the Elettra synchrotron (Trieste, Italy), using a 1.54 Å (8 keV) incidence X-ray beam. The sample was placed at 82.88 cm from a pixel detector (Pilatus 1M) on a rotation stage, which allowed setting of the glancing angle between the incident radiation and the sample to 90°.^[46] Samples were prepared on coverslips to allow measurements in Laue geometry. The angular scale of the detector was calibrated with Ag-behenate as the reference pattern.

Nanomechanical tests were performed using a triboindenter (Hysitron TI-950), equipped with a Berkovich tip and a 2D axis transducer. The value of the elastic modulus (E_r) was extracted from nanoindentation tests. Indentation measurements were performed 10 times using the partial load-unload function and Oliver–Pharr method^[47] and then corrected following the method described by Coy et al.^[48] Measurements were performed after 120 s of drift correction and shallow calibration (5–30 nm) of the indenter on commercially available fused quartz (69.6 GPa). Nanowear experiments were performed using double pass scans in a 10 × 10 μ m area in a constant load of 20 μ N. Total displaced material was calculated by the change of height between wear affected areas and pristine sections (10 × 10 μ m² (Δ Height_{(μ m)))). Nanowear and nanoscratch images were analyzed by built-in software and Gwyddion SPM software.}

Strontium Detection and Release Study: The presence of strontium was confirmed by X-ray photoelectron spectroscopy (XPS) atomic composition analysis. A SPECS Sage HR 100 spectrometer equipped with a 100 mm mean radius PHOIBOS analyzer and a non-monochromatic X-ray

source (Mg K_{α} line of 1253.6 eV energy and 250 W), placed perpendicular to the analyzer axis and calibrated using the $3d_{5/2}$ line of Ag, with a full width at half maximum of 1.1 eV was used. The selected resolution for high resolution spectra was 15 eV of pass energy and 0.15 eV per step. All measurements were made in an ultrahigh vacuum chamber at a pressure of around 8×10^{-8} mbar. An electron flood gun was used to neutralize charging. Measurements were conducted directly on the films, which were previously washed with absolute ethanol. The analysis of spectra was done with the CasaXPS 2.3.15dev87 software. Satellite removal and Shirley background subtraction were applied, the binding energies were calibrated assigning to the C 1s C – C peak 285 eV, and peaks were fitted with Gaussian – Lorentzian line shapes. Samples were measured in triplicate. To ensure the strontium is homogeneously distributed in the mesoporous titania, imaging was performed with a transmission electron microscope (TEM, JEOL JEM-2100F UHR, operated at 200 kV). A scanning transmission scanning microscope STEM-BF equipped with an EDX detector (Oxford INCA systems) was used for the semi-quantitative analysis of the film composition at different positions on the surface. INCA and Origin 2016 Pro software were used to analyze the data.

To measure the total amount of Sr in the SrTiMFs, the films were immersed in 5 mL HNO_3 >99.5% Puriss overnight (around 17 h) to complete dissolution of the film, then distilled water was added until a 5% concentration of HNO_3 was obtained for ICP-MS measurements. As a control, MTFs were also dissolved following the same procedure. Three samples for each film type were evaluated.

To study the release of Sr, samples were placed in wells of 12 multiwell dishes with 2 mL of 10 mM PBS and the Sr released was measured at 5, 15, 30 min, 1, 2, 6 h, and 1, 2, and 7 days. Samples were prepared in triplicate. The Sr released in 10 mM PBS was diluted to 5 mL in distilled water in 5% HNO_3 for ICP-MS measurements. The calibration curve for Sr was performed with 7 points ranging from 0 to 200 ppm; the curve was defined by the equation $y = 1.01x - 0.85$, where y is the measured intensity (a.u.) and x the Sr concentration (ppm) with an R^2 of 0.999. TEM images were acquired on samples previously immersed in 10 mM PBS for 24 h.

MC3T3-E1 Cell Bioactivity Experiments: To confirm cell adhesion to the substrates confocal laser scanning microscopy (Zeiss LSM510) images were taken after labeling of F-actin, focal adhesions and nuclei with an actin cytoskeleton and focal adhesion staining kit (FAK100, Millipore). Cell adhesion was evaluated on MTFs and SrTiMFs. Briefly, after reaching 80% confluence, cells were trypsinized and resuspended in fresh medium to a final cell density of 3×10^4 cells mL^{-1} . 1 mL of cell suspension was added into each well of 24 multiwell cell culture plates with the substrates. After culturing for 2 h, 24 h, 48 h and 7 days cells were fixed with a 4% paraformaldehyde solution. Cells were first permeabilized with Triton-X100 (Sigma–Aldrich) for 4 min at room temperature. Then, cells were incubated in dilute anti-vinculin primary antibody for 1 h at room temperature, followed by three washes for 5 – 10 min each with PBS with 0.05% Tween-20 (Sigma–Aldrich), followed by 1 h further incubation with a fluorescein isothiocyanate (FITC)-conjugated secondary antibody and tetramethylrhodamine (TRITC)-conjugated phalloidin at room temperature. After rinsing three times with wash buffer, cells were incubated with 4,6-diamidino-2-phenylindole (DAPI) for 3 min at room temperature, followed by three washes.

Cell proliferation was evaluated by colorimetric analysis using the Cell Counting Kit-8 (CCK-8, Sigma–Aldrich) containing WST-8 (2-[2-methoxy-4-nitrophenyl]-3-[4-nitrophenyl]-5-[2,4-disulphophenyl]-2H-tetrazolium, monosodium salt), a nontoxic dye used for continuous cell culturing. When cells reached 80% confluence, they were trypsinized and resuspended in fresh medium to a final cell density of 3×10^4 cells mL^{-1} . 1 mL of cell suspension was added into each well of 24 multiwell cell culture plates containing the substrates. Measurements were done in triplicate at 2 h, 1, 2, and 3 days. Cells cultured on the films were refreshed with 10% v/v of CCK-8 containing medium and after 2 h of incubation at 37 °C two aliquots of 100 μL of each sample were placed into a 96-well cell plate. Optical density of the reaction solution was acquired using a plate reader (GENios Pro, Tecan) equipped with a 450 nm filter.

For cell differentiation, osteogenic medium was used: full medium was supplemented with 50 $\mu\text{g mL}^{-1}$ of L-ascorbic acid and 2 mM of

β -glycerophosphate, both purchased from Sigma–Aldrich. Proliferating osteoblasts show greatly enhanced alkaline phosphatase activity in the stage of extracellular matrix maturation during bone formation in vitro. Alkaline phosphatase activity is therefore a well-recognized marker for osteoblast differentiation and mineralization.^[49] For alkaline phosphatase quantification, cells were seeded with a density of 5×10^4 cell mL^{-1} in a 24 multiwell dish. After 4 days of growth, concentrated osteogenic medium was added to obtain the desired concentration of L-ascorbic acid and β -glycerophosphate added. Cells were cultured in osteogenic medium for 20 days (adding 500 μL of medium every 4 days) following the differentiation over time. Alkaline phosphatase was quantified with the StemTAG™ Alkaline Phosphatase Activity Assay Kit from Cell Biolabs, Inc. This enzyme catalyzes the conversion of p-Nitrophenyl Phosphate (pNPP) to p-Nitrophenol (pN). p-Nitrophenol is a bright yellow-colored compound which has maximum absorbance at 405 nm. The rate of absorbance increment from pNPP (colourless) to pN (color) is directly proportional to the AP enzyme activity in the serum sample. Following the indications of the manufacturer, a 10-point calibration curve with pN at concentrations ranging from 0.5 mM to 0.9766 μM was measured and defined as $y = 0.04 + 7.51x$, where y is the absorbance at 405 nm and x is the pN in mM with an R^2 of 0.999. Cells were cleaned twice with PBS and lysated with 250 μL lysis buffer for 10 min at 4 °C. The cell debris was centrifuged at 12,000g for 10 min. The supernatant was mixed in a 1:1 volume ratio with pNPP and was incubated for 15 min at 37 °C. To stop the reaction the same proportion in volume of 1× stop solution was added and shaken for 30 s.

The Bradford assay was performed to quantify the protein concentration in the lysate. For the assay, 1 part of protein sample was mixed with 30 parts of the Bradford reagent, which consists of a dye, Brilliant Blue G that forms a complex with proteins, shifting the absorption maximum from 465 to 595 nm. Bovine serum albumin (BSA), from Sigma, was used as a protein standard. The calibration curve with 5 points ranging from 1 to 2 mg mL^{-1} of BSA was defined as $y = 0.37 + 0.13x$ where y is the absorbance at 595 nm and x is the total amount of protein in mg mL^{-1} with an R^2 of 0.983. Absorbance measurements were performed with a Thermo Scientific™ Varioskan™ Flash Multimode Reader.

All the ANOVA statistical analyses were done using OriginPro 2016 software.

Supporting Information

Supporting Information is available from the Wiley Online Library or from the author.

Acknowledgements

The authors thank the MAT2017-88752-R Retos project from the Ministerio de Economía, Industria y Competitividad, gobierno de España for support. This work was performed under the Maria de Maeztu Units of Excellence Program from the Spanish State Research Agency – Grant No. MDM-2017-0720. The authors also thank Dr. Julia Cope for her revision of the manuscript. The authors acknowledge the CERIC-ERIC consortium for the access to experimental facilities at the Elettra synchrotron (Trieste) and the financial support.

Conflict of Interest

The authors declare no conflict of interest.

Keywords

strontium titanate, mesoporous thin films, pre-osteoblasts, osseointegration

Received: November 13, 2018

Revised: May 22, 2019

Published online:

- [1] L. C. Jones, L. D. Timmie Topoleski, A. K. Tsao, *Mechanical Testing of Orthopaedic Implants*, Woodhead Publishing, Elsevier, Sawston, Cambridge, United Kingdom **2017**, pp. 17–32.
- [2] M. Navarro, A. Michiardi, O. Castano, J. Planell, *J. R. Soc. Interface* **2008**, *5*, 1137.
- [3] M. Geetha, A. K. Singh, R. Asokamani, A. K. Gogia, *Prog. Mater. Sci.* **2009**, *54*, 397.
- [4] A. Kertmen, E. Barbé, M. Szkoda, K. Siuzdak, V. Babačić, P. Torruella, M. Kotkowiak, S. Estradé, F. Peiró, S. Jurga, Y. Li, E. Coy, *Adv. Mater. Interfaces* **2019**, *6*, 1801286.
- [5] K. Karthik, S. Sivaraj, V. Thangaswamy, *J. Pharm. Bioallied Sci.* **2013**, *5*, S117.
- [6] J. Lawrence Katz, *Nature* **1980**, *288*, 196.
- [7] C. N. Elias, J. H. C. Lima, R. Valiev, M. A. Meyers, *JOM* **2008**, *60*, 46.
- [8] X. Song, W. Tang, D. Gregurec, L. Yate, S. E. Moya, G. Wang, *Appl. Surf. Sci.* **2018**, *436*, 653.
- [9] M. Echeverry-Rendón, O. Galvis, R. Aguirre, S. Robledo, J. G. Castaño, F. Echeverría, *J. Mater. Sci. Mater. Med.* **2017**, *28*, 169.
- [10] W. Chen, X. Shen, Y. Hu, K. Xu, Q. Ran, Y. Yu, L. Dai, Z. Yuan, L. Huang, T. Shen, K. Cai, *Biomaterials* **2017**, *114*, 82.
- [11] X. Liu, P. Chu, C. Ding, *Mater. Sci. Eng. R Rep.* **2004**, *47*, 49.
- [12] J. D. Bass, D. Grosso, C. Boissiere, E. Belamie, T. Coradin, C. Sanchez, *Chem. Mater.* **2007**, *19*, 4349.
- [13] Z. Xu, H. Lu, J. Lu, C. Lv, X. Zhao, G. Wang, *RSC Adv.* **2018**, *8*, 3051.
- [14] X. Song, W. Tang, D. Gregurec, L. Yate, S. E. Moya, G. Wang, *Appl. Surf. Sci.* **2018**, *436*, 653.
- [15] E. O'Neill, G. Awale, L. Daneshmandi, O. Umerah, K. W.-H. Lo, *Drug Discov. Today* **2018**, *23*, 879.
- [16] W. Zhang, G. Wang, Y. Liu, X. Zhao, D. Zou, C. Zhu, Y. Jin, Q. Huang, J. Sun, X. Liu, X. Jiang, H. Zreiqat, *Biomaterials* **2013**, *34*, 3184.
- [17] P. Habibovic, J. E. Barralet, *Acta Biomater.* **2011**, *7*, 3013.
- [18] P. J. Marie, P. Ammann, G. Boivin, C. Rey, *Calcif. Tissue Int.* **2001**, *69*, 121.
- [19] A. L.-J. Liu, P.-W. Shen, P.-J. Chen, *Clin. Cases Miner. Bone Metab.* **2013**, *10*, 206.
- [20] L. Maimoun, T. C. Brennan, I. Badoud, V. Dubois-Ferriere, R. Rizzoli, P. Ammann, *Bone* **2010**, *46*, 1436.
- [21] M. J. Bolland, A. Grey, *BMJ* **2016**, *354*, 5109.
- [22] V. Offermanns, O. Z. Andersen, G. Riede, M. Sillassen, C. S. Jeppesen, K. P. Almqvist, H. Talasz, C. Öhman-Mägi, B. Lethaus, R. Tolba, F. Kloss, M. Foss, *Acta Biomater.* **2018**, *69*, 385.
- [23] F. Yang, D. Yang, J. Tu, Q. Zheng, L. Cai, L. Wang, *Stem Cells* **2011**, *29*, 981.
- [24] C. Zhou, A. Xu, D. Wang, G. Lin, T. Liu, F. He, *Biomater. Sci.* **2018**, *6*, 1946.
- [25] N. Li, L. Zhang, Y. Chen, M. Fang, J. Zhang, H. Wang, *Adv. Funct. Mater.* **2012**, *22*, 835.
- [26] C. Zhou, A. Xu, D. Wang, G. Lin, T. Liu, F. He, *Biomater. Sci.* **2018**, *6*, 1946.
- [27] M. Vallet-Regí, M. Manzano Garcia, M. Colilla, *Biomedical Applications of Mesoporous Ceramics: Drug Delivery, Smart Materials, and Bone Tissue Engineering*, CRC Press, Indianapolis, IN **2012**.
- [28] T. Rahman, R. Liu, E. Ortel, R. Kraehnert, A. Antoniou, *Appl. Phys. Lett.* **2014**, *104*, 241902.
- [29] C. Boissiere, D. Grosso, S. Lepoutre, L. Nicole, A. Aline, B. Bruneau, C. Sanchez, *Langmuir* **2005**, *21*, 12362.
- [30] K. Grandfield, S. Pujari, M. Ott, H. Engqvist, W. Xia, *J. Biomater. Nanobiotechnol.* **2013**, *04*, 107.
- [31] E. Nielsen, K. Greve, O. Ladefoged, *Strontium, Inorganic and Soluble Salts Evaluation of Health Hazards and Proposal of Health Based Quality Criteria for Drinking Water*, The Danish Environmental Protection Copenhagen, Denmark **2013**.
- [32] D. F. Jacques, B. I. Bourland, *Soc. Pet. Eng. J.* **1983**, *23*, 292.
- [33] C. Christgau, H. Hansen, J. Nilsson, S. Andersen, *Water-Soluble Strontium Salts for Use in Treatment of Cartilage and/or Bone Conditions*, Osteologix A/S Glen Allen, Virginia, USA **2003**.
- [34] D. Grosso, C. Boissiere, B. Smarsly, T. Brezesinski, N. Pinna, P. A. Albouy, H. Amenitsch, M. Antonietti, C. Sanchez, *Nat. Mater.* **2004**, *3*, 787.
- [35] A. Escobar, L. Yate, M. Grzelczak, H. Amenitsch, S. E. Moya, A. V. Bordoni, P. C. Angelome, *ACS Omega* **2017**, *2*, 4548.
- [36] D. F. Lionello, P. Y. Steinberg, M. M. Zalduendo, G. J. A. A. Soler-Illia, P. C. Angelomé, M. C. Fuertes, *J. Phys. Chem. C* **2017**, *121*, 22576.
- [37] J. L. Vivero-Escoto, Y.-D. Chiang, K. Wu, Y. Yamauchi, *Sci. Technol. Adv. Mater.* **2012**, *13*, 013003.
- [38] A. L. Sangle, S. Singh, J. Jian, S. R. Bajpe, H. Wang, N. Khare, J. L. MacManus-Driscoll, *Nano Lett.* **2016**, *16*, 7338.
- [39] M. G. Bellino, S. Golbert, M. C. De Marzi, G. J. A. A. Soler, *Biomater. Sci.* **2013**, *1*, 186.
- [40] Z. Zhang, B. Gu, W. Zhu, L. Zhu, *Exp. Ther. Med.* **2013**, *6*, 707.
- [41] J. D. Humphries, P. Wang, C. Streuli, B. Geiger, M. J. Humphries, C. Ballestrem, *J. Cell Biol.* **2007**, *179*, 1043.
- [42] K. A. DeMali, *Trends Biochem. Sci.* **2004**, *29*, 565.
- [43] K. Anselme, *Biomaterials* **2000**, *21*, 667.
- [44] J. Shi, Y. Li, Y. Gu, S. Qiao, X. Zhang, H. Lai, *Sci. Rep.* **2017**, *7*, 15563.
- [45] M. Murshed, D. Harmey, J. L. Millán, M. D. McKee, G. Karsenty, *Genes Dev.* **2005**, *19*, 1093.
- [46] H. Amenitsch, S. Bernstorff, M. Kriechbaum, D. Lombardo, H. Mio, M. Rappolt, P. Laggner, *IUCr, J. Appl. Crystallogr.* **1997**, *30*, 872.
- [47] W. C. Oliver, G. M. Pharr, *J. Mater. Res.* **1992**, *7*, 1564.
- [48] E. Coy, L. Yate, Z. Kabacińska, M. Jancelewicz, S. Jurga, I. Iatsunskyi, *Mater. Des.* **2016**, *111*, 584.
- [49] M. Weinreb, D. Shinar, G. A. Rodan, *J. Bone Miner. Res.* **2009**, *5*, 831.